Improving Safety and Accuracy of Impedance Controlled Robot Manipulators with Proximity Perception and Proactive Impact Reactions

Conference Paper · May 2021

DOI: 10.1109/ICRA48506.2021.9561025

2 authors:

Yitao Ding
Technische Universität Chemnitz
15 PUBLICATIONS **140** CITATIONS

SEE PROFILE

Ulrike Thomas
Technische Universität Chemnitz
52 PUBLICATIONS **409** CITATIONS

SEE PROFILE

Improving Safety and Accuracy of Impedance Controlled Robot Manipulators with Proximity Perception and Proactive Impact Reactions

Yitao Ding and Ulrike Thomas

***Abstract*— We present a system which improves the safety and accuracy of impedance controlled robotic manipulators with proximity perception. Proximity servoed manipulators, which use proximity sensors attached to the robot's outer shell, have recently demonstrated robust collision avoidance abilities. Nevertheless, unwanted collisions cannot be avoided entirely. As a fallback safety mechanism, robots with joint force/torque sensing rely on impedance controllers for impact attenuation and compliant behavior. However, impedance controllers induce undesired deflections of the robot from its trajectory when it is not in contact. These deviations are more pronounced at soft configurations and when the robot grasps objects of unknown weight distribution, thus a compromise must be made between high positional accuracy and softness (safety). The proximity information allows the robot to react to anticipated impacts proactively for attenuation and damage reduction of unavoidable collisions, while still maintaining high accuracy during regular operation. This is achieved through variations of impedance parameters according to proximity measurements and motions towards safe joint configurations during the pre-impact phase.**

I. Introduction

In applications involving collaboration between humans and robotic manipulators, safety is of the highest priority. A high level of safety is achievable through collision avoidance, where undesired contacts between robots and humans are avoided at all. Fast and occlusion free perception is fundamental for collision avoidance. However, undesired contacts will always occur and can not be entirely avoided even with perfect perception. We propose using proximity perception to leverage the pre-impact phase allowing the robot to react proactively to anticipated and unavoidable contacts. In this phase, the robot's compliance is increased to render low inertia and soft behavior for enhanced safety, similar to virtual airbags and soft skins [1]. While in regular operation, the robot is less reactive to external force disturbances to increase accuracy. Furthermore, through reactive motions to safe joint configurations, more joints can contribute to reducing the inertia and attenuating impacts.

Safety specifications, such as ISO/TS 15066, specify safety requirements for collaborative working cells at different collaboration levels to minimize damages and injuries from collisions. The standards rely mainly on two regimes for close collaboration, maintaining safety distance and limiting force, pressure, and energy transferred to the human body. The second method mainly applies to backdrivable robots with soft joints, either mechanically or through impedance control [2] with force/torque sensors in the joints. Impedance controlled robots emulate a virtual spring-mass-damper system, and external forces can deflect the manipulator to achieve compliant behavior. Hence, impedance control is used as a second safety layer to attenuate impact through the robot's compliance after collision avoidance failure. The aim is to render low inertia and spring stiffness for improved compliance and increased safety. The current control paradigm for impedance controlled robots is: Stiff and slow, fast and soft [3] to maintain the maximum allowed force thresholds transferred to the human body, which is very restrictive. In addition, the calculation of external forces is subject to disturbances caused by the compensation of intrinsic forces (inaccuracies in the robot's dynamic model), unknown weight distribution of picked up objects, and the joint force/torque measurement itself. It is particularly noticeable during regular contactless operation and lower spring stiffness where the robot is more reactive to external forces – disturbances in the intrinsic force estimation cause undesired deflections from the robot's path. Therefore a contradiction between positional accuracy (stiff) and safety (soft) exists.

De Luca et al. [4] identified three significant phases during impact, which are: pre-impact, impact, and post-impact phase. Different measures in each phase can attenuate impact. In the first pre-impact phase, obstacles are sensed and counteracted, e.g. by avoiding undesired collision,

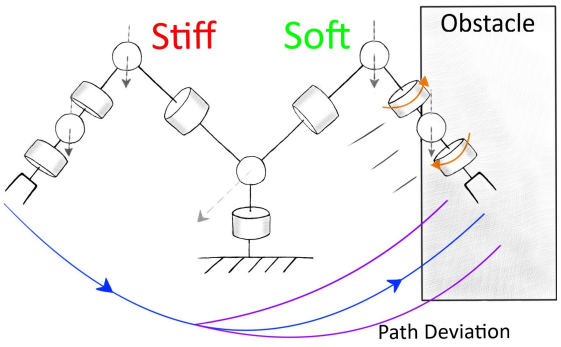

Fig. 1. The high position accuracy remains when the robot is in regular operation. The accuracy only decreases when the joint stiffness is reduced due to obstacles detected by proximity sensors. The robot also increases the manipulability at the contact point in contact direction for more effective impact attenuation.

The authors are with the Lab of Robotics and Human-Machine-Interaction at Chemnitz University of Technology, 09126 SN Chemnitz, Germany. Emails: {yitao.ding, ulrike.thomas}@etit.tu-chemnitz.de

to ensure safety. When contact occurs, mechanical design measures can reduce damage, such as a lightweight design with rounded shapes, soft elastic covers, and elastic joints. Elastic joints can be either mechanical driven or realized by impedance control. In the post-impact phase, the robot has to detect the collision occurrence and react appropriately with a recovery strategy [5].

We think that further investigation and exploitation of the pre-impact phase, apart from collision avoidance, offer greater potential to minimize injuries. Robot manipulators equipped with proximity sensors on their outer shell offer fast perception capabilities of obstacles due to the minimum amount of relevant data to represent obstacles and the absence of redundant information, such as provided from exteroceptive 3D cameras. Compared to 3D cameras, proximity perception also does not suffer from occlusion with their inside-out view concept and can be used to anticipate impacts. With their properties, they allow the robot to react quickly to obstacles in a reflex-like way not only for collision avoidance [6] [7] but also to proactively perform measures during the pre-impact phase for unavoidable collisions.

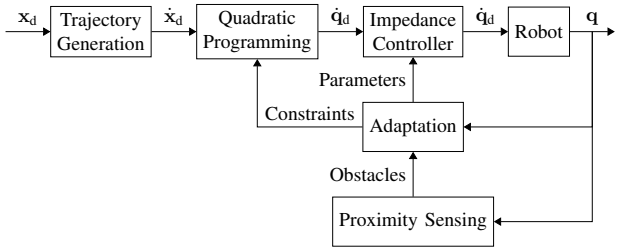

Fig. 2. Extension of our prior introduced reactive motions framework for collision avoidance with safe joint configuration motions. The impedance parameters are adjusted for impact attenuation during pre-contact and accuracy during normal operation.

In this paper, we increase safety, accuracy, and maximum allowed velocity by leveraging the pre-impact phase with proximity perception in two ways. First, we use proximity information to adjust the impedance controller's parameters, which renders only low inertia when needed and thus keeping high accuracy in the main task. Second, to gain maximum utilization of the joint compliance, the robot moves to safe robot joint configurations before unavoidable contacts occur. To the best of our knowledge, this is the first approach that uses proximity sensors to modulate the robot's impedance and to generate motions to safe joint configurations.

As Fig. 2 illustrates, obstacles are detected through proximity sensors on the robot's outer shell. We extend our prior introduced reactive motion framework for collision avoidance based on constrained quadratic optimization [7] to incorporate pre-impact reactions. Generally, collision avoidance allows for faster robot motions in human-robot collaboration scenarios, as the robot can avoid obstacles or reduce velocities before to impact. The pre-impact phase is triggered when obstacles are or will become too close. During this period, the robot starts to soften its joint stiffness. It allows us to overcome conventional impedance control limitations to increase both safety and accuracy as required. The stiffness modulation is governed by an energy-tank based control law, which ensures stability during increases in stiffness. At the same time, the manipulability at the anticipated contact point is increased towards the obstacle direction. The manipulability is weighted, with joints closer to the anticipated impact position having greater weights, which effectively decreases inertia mechanically during impact. A proactive motion is generated towards joint configurations where a larger number of joints can attenuate the impact, thereby increasing the effectiveness of the robot's impedance controller.

II. Related Work

The dynamic adjustment of impedance parameters is referred to as variable impedance/admittance control (VIC/VAC) and is often used to increase the performance and stability of conventional impedance controllers. Müller et al. [8] combined VIC with artificial potential fields for hand-guided robot applications. The parameters are adjusted to increase the intuitiveness while the robot is guided along a predefined path. Since hand-held end-effectors change the dynamics of the kinematic chain and can behave non-passively, the stability of such systems can decrease. Ficuciello et al. [9] adjusted the damping parameters to increase hand guidance accuracy. Also, during collisions with high stiffness environments, impedance controllers have stability issues. Ferraguti et al. [10] proposed a method to detect instability and adapt the parameters to restore stability.

Impact attenuation with compliance behavior relies mostly on soft padding materials on the robot's surface, mechanical variable stiffness joints, or virtual impedance control with force/torque sensors. Common reaction mechanisms include techniques for detecting impacts and their occurrence to trigger and adjust the soft joint behavior. De Luca et al. [11] proposed two modes of operation for a high-performance controller for physical human-robot interaction. During co-existence, no contact is allowed with collision avoidance. Limited contact is only permitted between specific parts between humans and robots. For unavoidable collisions, force/torque sensors in the robot's joint detect and isolate the impact and trigger admittance control and acceleration motions away from the obstacle. These measures are only activated after the impact has already occurred. Schiavi et al. [3] attenuate impacts on a 3-DoF manipulator with elastic joints based on McKibben muscles. At the same time, the authors achieved higher precision and safety by adjusting the joints stiffness after an impact has been detected. Fernandez et al. [12] also proposed to switch from velocity to impedance control after impact detection. They emphasized the difficulty in detection due to the short collision period and the occurrence of instabilities of the impedance controller after collision with stiff environments due to the fast reaction timing requirements.

The ability to sense obstacles in proximity provides pre-knowledge and can solve issues associated with pure joint force measurements. The pre-knowledge gives the robot

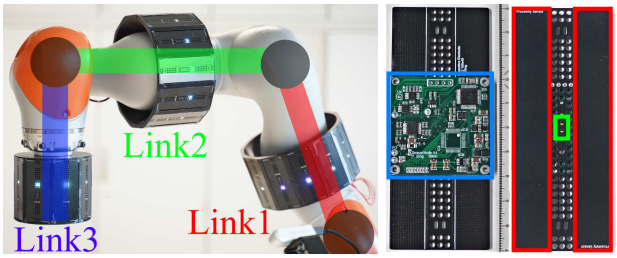

(a) (b)

Fig. 3. a) Proximity servoing system with three proximity sensing cuffs. b) The sensing modules on the cuff use time-of-flight (green) and electric field (red) for narrow-far and wide-near field proximity measurements.

enough time to generate proactive, reactive motions and to adjust control parameters. Chun et al. [13] exploit proximity perception from RGBD-cameras for collision avoidance based on artificial potential fields and generate safe joint configurations [14] to attenuate potential collision. They align the joints towards the collision to improve the effectiveness of their variable stiffness joints.

III. Proximity Servoing Fundamentals

A. Proximity Perception

We use the proximity servoed robot system from our previous collision avoidance work [6]. In short, the system comprises of three proximity sensing cuffs attached on a 7-dof Kuka LBR iiwa 7 R800 (Fig. 3). Two cuffs on the lower link house twelve proximity sensing modules each and the cuff on the TCP has eight sensing modules. The arrangement of the sensing elements within the cuffs provide 360° of view. The proximity sensors [15] use time-of-flight (ToF) based laser range sensors for far-field measurements up to $1\,\mathrm{m}$ and capacitive sensors to cover the wide close range area around the robot, where the ToF sensors are blind. The capacitive measurements do not provide quantitative information and are highly affected by material properties. Therefore, obstacles only trigger binary signals when certain thresholds are exceeded. The signals form virtual objects with a constant range in close distance. In the end, the proximity sensing system provides a point cloud in the robot base coordinate system of which the minimum distances to the links of the robots are calculated.

B. Proximity Servoed Reactive Motion

The proximity servoed motion is generated by utilizing our reactive collision avoidance framework based on constrained quadratic programming [7].

$$\min_{\dot{\mathbf{q}}} \frac{1}{2}\dot{\mathbf{q}}^{\mathsf{T}}\mathbf{H}\dot{\mathbf{q}} + f^{\mathsf{T}}\dot{\mathbf{q}} \quad \text{s.t.} \begin{cases} \mathbf{A}\dot{\mathbf{q}} \leq \mathbf{b}, \\ \mathbf{b}_{\mathrm{l}} \leq \dot{\mathbf{q}} \leq \mathbf{b}_{\mathrm{u}} \end{cases} \tag{1}$$

$$\mathbf{H} = \mathbf{J}^{\mathsf{T}}\mathbf{J} + \mathrm{diag}\,(\mathbf{w}_1) \qquad f_1 = -\dot{\mathbf{x}}^{\mathsf{T}}\mathbf{J} \tag{2}$$

$$\mathbf{A} = \begin{bmatrix} \hat{\mathbf{s}}^{\mathsf{T}}\mathbf{J}_{\mathrm{c}} \\ -\mathbf{J}_{\mathrm{a}} \end{bmatrix} \qquad \mathbf{b} = \begin{bmatrix} \dot{\mathbf{x}}_{\mathrm{a}} \\ 0 \end{bmatrix} \tag{3}$$

$$\mathbf{b}_{\mathrm{l}} = \begin{cases} 0, & \mathbf{q} \leq \mathbf{q}_{\mathrm{lb}} \\ \dot{\mathbf{q}}_{\mathrm{lb}}, & \text{otherwise} \end{cases} \qquad \mathbf{b}_{\mathrm{u}} = \begin{cases} 0, & \mathbf{q} \geq \mathbf{q}_{\mathrm{ub}} \\ \dot{\mathbf{q}}_{\mathrm{ub}}, & \text{otherwise} \end{cases} \tag{4}$$

$\mathbf{J}$ is the end-effector Jacobian and its inverse maps the commanded task motion $\dot{\mathbf{x}}$ to joint motions $\dot{\mathbf{q}}$. $\mathbf{H}$ and f represent the quadratic and linear objective term and minimize the quadratic motion error $e = \frac{1}{2}\left(\dot{\mathbf{x}} - \mathbf{J}\dot{\mathbf{q}}\right)^{\mathsf{T}}\left(\dot{\mathbf{x}} - \mathbf{J}\dot{\mathbf{q}}\right)$. $\mathbf{A}$ and $\mathbf{b}$ are the linear inequality constraints created by obstacles in proximity. The constraints limit the approach velocity $\dot{\mathbf{x}}_{\mathrm{a}} > \hat{\mathbf{s}}^{\mathsf{T}}\mathbf{J}_{\mathrm{c}}\dot{\mathbf{q}}$ towards obstacles, where $\hat{\mathbf{s}}$ is the direction vector pointing from the anticipated collision point on the manipulator to the obstacle and $\mathbf{J}_{\mathrm{c}}$ the Jacobian of the anticipated collision point. $\mathbf{J}_{\mathrm{a}}$ is the Jacobian of the weighted summmed distance of all obstacles. The constraint $-\mathbf{J}_{\mathrm{a}}\dot{\mathbf{q}} < 0$ actively increases distances towards obstacles for motions around obstacles. $\mathbf{b}_{\mathrm{l}}$ and $\mathbf{b}_{\mathrm{u}}$ limit the joint angles to lower and upper bounds.

IV. Variable Impedance Control

A. Stability

As contacts on the robot can occur on any link, the robot's impedance is controlled in joint space. First, let us assume the standard impedance control law with constant parameters:

$$\boldsymbol{\tau}_{\mathrm{ext}} = \mathbf{K}_{\mathrm{d}}\tilde{\mathbf{q}} + \mathbf{D}_{\mathrm{d}}\dot{\tilde{\mathbf{q}}} + \mathbf{M}_{\mathrm{d}}\ddot{\tilde{\mathbf{q}}} \tag{5}$$

where $\mathbf{K}_{\mathrm{d}}$, $\mathbf{D}_{\mathrm{d}}$, and $\mathbf{M}_{\mathrm{d}}$ are the desired stiffness, damping, mass parameters. $\tilde{\mathbf{q}}$ are the joint deflections from the desired configuration, and $\boldsymbol{\tau}_{\mathrm{ext}}$ the resulting forces and torques. This part relies on the work of Ferraguti et al. [16], who showed that this type of control law behaves passively and thus stable. However, when the stiffness parameter $\mathbf{K}_{\mathrm{d}}(t)$ becomes variable, passivity can potentially be violated, as shown by the first time derivative of the Lyapunov candidate.

$$\dot{V} = \dot{\tilde{\mathbf{q}}}^{\mathsf{T}}\boldsymbol{\tau}_{\mathrm{ext}} + \left[\frac{1}{2}\,\tilde{\mathbf{q}}^{\mathsf{T}}\dot{\mathbf{K}}_{\mathrm{d}}\tilde{\mathbf{q}} - \dot{\tilde{\mathbf{q}}}^{\mathsf{T}}\mathbf{D}_{\mathrm{d}}\dot{\tilde{\mathbf{q}}}\right] \leq 0 \tag{6}$$

In the brackets in (6), the first term can become positive definite and thus an energy source with non-passive behavior. Violations can occur when the robot is strongly deflected from the desired joint configuration and when the robot increases its stiffness during low damping. This can be interpreted as an increase of stored potential energy with limited dissipation capabilities since the deflection remains the same for a higher spring stiffness. On the other hand, the system remains passive during a decrease in stiffness. It allows us to assume that the robot behaves stable when adjusting its stiffness parameter to low stiffness and low damping during pre-impact detection. Problems arise during false-positive pre-impact detections and the recovery of the original stiffness parameters without violating passivity. Ferraguti et al. proposed using energy tank-based impedance control introduced by Duindam et al. [17] to ensure the stability of variable impedance systems. The additional energy

storing element in the impedance model stores the damping element's dissipated energy in a virtual energy tank. The stored energy can then be used for non-passive actions until all energy is used up. From the outside, the system remains passive. The energy tank dynamics are as follows:

$$\dot{x}_\mathrm{t} = \frac{\sigma}{x_\mathrm{t}} \left(\dot{\tilde{\mathbf{q}}}^\mathsf{T} \mathbf{D}_\mathrm{d} \dot{\tilde{\mathbf{q}}} \right) - \mathbf{w}^\mathsf{T} \dot{\tilde{\mathbf{q}}} \tag{7}$$

where x_t describes the energy level $T = \frac{1}{2} x_\mathrm{t}^2$ of the tank. The fill and discharge rate is modelled with:

$$\sigma = \begin{cases} 1, & T(x_\mathrm{t}) \leq \bar{T} \\ 0, & \text{otherwise} \end{cases} \tag{8}$$

$$\mathbf{w} = \begin{cases} -\frac{\mathbf{K}_\mathrm{d} \tilde{\mathbf{q}}}{x_\mathrm{t}}, & T(x_\mathrm{t}) > \varepsilon \\ 0, & \text{otherwise} \end{cases} \tag{9}$$

σ prevents overfill of the tank above $\bar{T}$. The tank is additionally limited to stay within $\bar{T}$ and ε. $\mathbf{w}$ sources the energy to change the stiffness $\mathbf{K}_\mathrm{d}$ as long as $T(x_\mathrm{t}) > \varepsilon$ is not depleted $> \varepsilon$, otherwise $\mathbf{K}_\mathrm{d}$ remains constant in order to maintain stability.

B. Impedance Parameter Control for Impact Attenuation

To maintain the accuracy of position control during regular operation, the stiffness parameters are only reduced when impacts are likely to happen. Since with proximity sensors we exchange spatial resolution for fast low latency perception, tracking and predicting obstacle trajectories are not feasible due to the limited number of measurement points. Therefore in our approach, the impedance parameters $\mathbf{K}_\mathrm{d}$ change as a function of obstacle distance (Fig. 4). Of course, if tracking is possible, more sophisticated impact prediction algorithms can be integrated that incorporate the obstacle velocity.

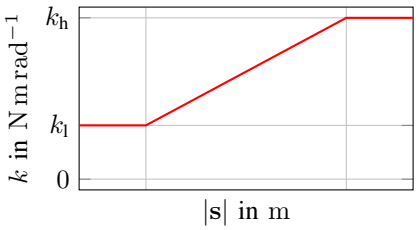

Fig. 4. Torsional spring constant k vs. obstacle distance $|\mathbf{s}|$.

We control the slew rate of the stiffness, as illustrated in Fig. 5. The positive and negative slew rates are individually limited. It is desired to switch immediately from high stiffness to lower values once contact is predicted. Although the energy tank keeps the system stable, unpredictable behavior, such as sudden acceleration, may still occur with the remaining energy in the tank. For predictable behavior, the positive slew rate is limited to allow a slow rise in stiffness parameters during the recovery of the original robot state.

V. Safe Joint Configuration

The robot changes its joint configuration proactively in order to achieve highest impact attenuation effectiveness of

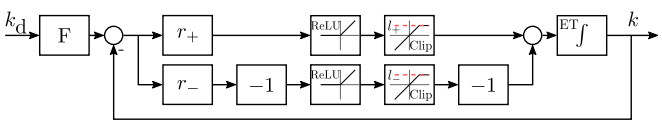

Fig. 5. Stiffness control with individual stiffness slew rate limitations during increase and decrease. The energy tank passes through the stiffness change to the integrator if the tank has enough energy to ensure stability.

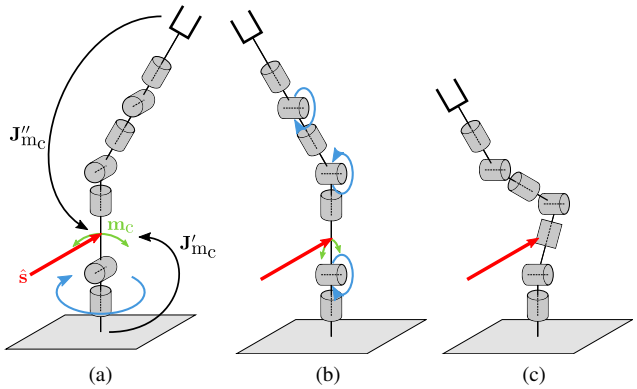

Fig. 6. a) Reduced impact attenuation with impedance control in the initial joint configuration, since the main manipulability direction at the anticipated contact point is tangential to the impact direction $\hat{\mathbf{s}}$. b) A motion towards safe joint configurations increases the attenuation capabilities. c) During impact, the impedance controller performs compliant motions.

the impedance controller. As illustrated in Fig. 6, the main goal is to move the joints to become more effective for the impedance controller. To create this kind of motion, we maximize the manipulability in the collision direction at the anticipated contact point on the robot with respect to each joint. This is achieved with an additional linear minimization/maximization term to the existing quadratic program for collision avoidance. Implementing a minimization/maximization term is essential, as the remaining constraints for collision avoidance are still active, which prohibits unsafe configurations and motions towards existing obstacles.

First, we use the position Jacobian $\mathbf{J}'_\mathrm{c} \in \mathbb{R}^{3\times i}$ at the impact point $\mathbf{c}$ to calculate the manipulability $\mathbf{m}'_\mathrm{c} \in \mathbb{R}^i$ in the direction of impact $\hat{\mathbf{s}}$ for all 1 to i joints, where the impact location is at the i-th link/joint.

$$\mathbf{m}'_\mathrm{c} = \frac{1}{2} \left(\mathbf{J}'^\mathsf{T}_\mathrm{c} \hat{\mathbf{s}} \right) \circ \left(\mathbf{J}'^\mathsf{T}_\mathrm{c} \hat{\mathbf{s}} \right) \tag{10}$$

The proposed manipulability metric $\mathbf{m}'_\mathrm{c}$ differs slightly from the manipulability proposed by Yoshikawa [18] and Nakamura et al. [19] as it only represents the manipulability of a point on the manipulator towards a certain direction, away from the collision. We then compute $\mathbf{J}'_{\mathrm{m_c}}$, which is the derivative of each element in $\mathbf{m}_\mathrm{c}$ with respect to joint positions $\mathbf{q}$. $\mathbf{J}'_{\mathrm{m_c}}$ describes how each joint position affects the manipulability. The computation can be done numerically or analytically as shown in Appendix I.

$$\mathbf{J}'_{\mathrm{m_c}} = \nabla_\mathbf{q} \mathbf{m}'_\mathrm{c} \tag{11}$$

When a contact occurs on link i, only joints 1 to i influence the manipulability $\mathbf{m}_c'$. However as shown in Fig. 6c, the remaining $i+1$ to n joints can contribute to attenuation as well. Therefore we further compute $\mathbf{J}''_{m_c}$, which is the same Jacobian with the end-effector as the root of the kinematic chain. In other words, the end-effector is assumed as static, while the base as free moving. With $\mathbf{J}_{m_c}^{\mathsf{T}} = \begin{bmatrix}\mathbf{J}_{m_c}'^{\mathsf{T}} & \mathbf{J}_{m_c}''^{\mathsf{T}}\end{bmatrix}$, we can summarize all joints within a single Jacobian $\mathbf{J}_{m_c}$ to increase impact attenuation with all joints.

We can then extend (2) with the additional weighted minimization term. The weights $\mathbf{w}_2$ allow us to assign higher priority to joints that are closer to the anticipated contact points which reduces inertia.

$$\mathbf{H} = \mathbf{J}^{\mathsf{T}}\mathbf{J} + \operatorname{diag}(\mathbf{w}_1) \qquad f_2 = -\dot{\mathbf{x}}^{\mathsf{T}}\mathbf{J} - \mathbf{w}_2^{\mathsf{T}}\mathbf{J}_{m_c} \tag{12}$$

The goal is to increase manipulability only slightly to reduce unpredictable behavior and effects on the TCP motion, therefore $\mathbf{w}_2$ is kept low.

VI. Experimental Results

We have performed two experiments for safe joint configuration motions and variable joint stiffness to evaluate the algorithms. In both experiments, the robot moves in a straight line to a target position where an obstacle is located at a distance of $0.1\,\mathrm{m}$. Collision avoidance is turned off to prevent avoidance motions. During the variable joint stiffness test, the robot has an additional weight of $0.25\,\mathrm{kg}$ at the TCP to reproduce a grasped object with unknown weight distribution. The weight amplifies the position error when modulating high and low stiffness values and highlights the effectiveness of the variable impedance approach in achieving high accuracy during regular operation. The joint stiffness range is modulated from 25 to $1000\,\mathrm{N\,m\,rad^{-1}}$ within the distance of 0.15 to $0.3\,\mathrm{m}$, similar to Fig. 4.

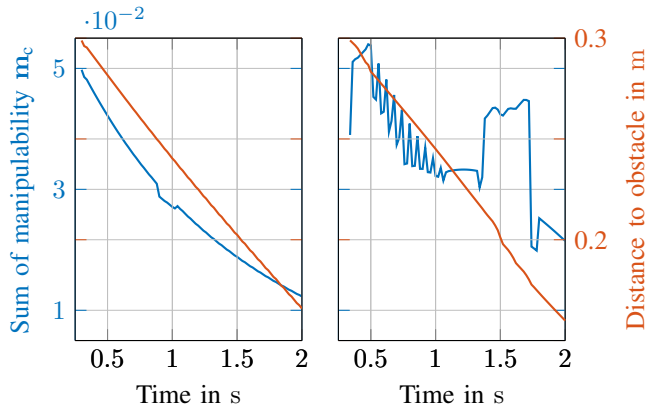

Fig. 7. Progress of manipulability $\mathbf{m}_c$ with safe joint configurations turned off (a) and on (b).

Fig. 7 shows the manipulability $\mathbf{m}_c$ with respect to obstacle distance $|\mathbf{s}|$ when safe joint configuration motions are deactivated and activated. $\mathbf{m}_c$ decreases fast over time when safe joint configuration motions are deactivated, which leads to more substantial inertia at the impact point. However, when activated, $\mathbf{m}_c$ decreases slower, which means that the inertia of the other robot links are weaker coupled to the link where the impact occurs. Therefore, the impedance controllers within each joint contribute slightly more to attenuating impacts. Since the task motion error is minimized and not defined as constrained, the task motion is marginally affected by the safe joint configuration motions. They are generally weighted lower than the task motion error to avoid unpredictable behavior. A compromise must be found where the overall path deviations and the contact point's path deviation are acceptable compared to the gain in manipulability.

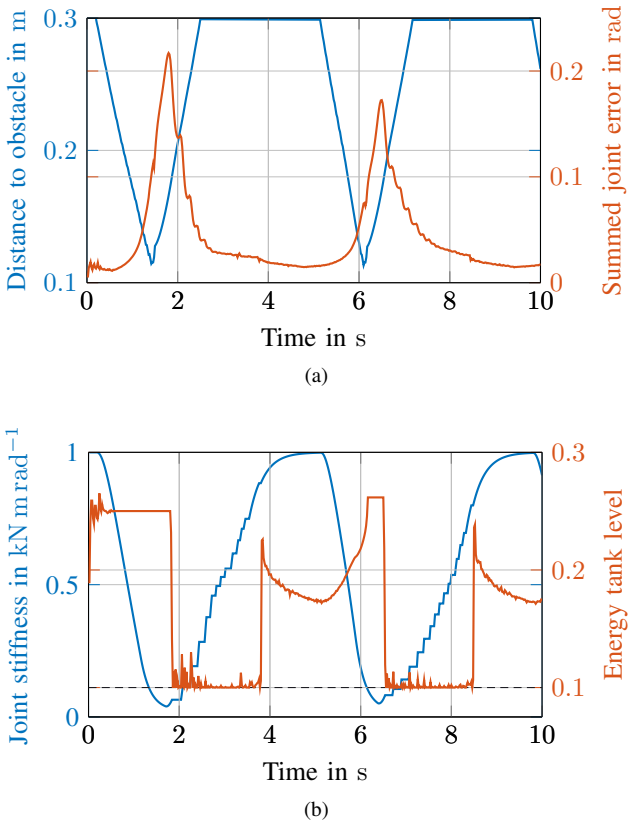

Fig. 8. a) Distance to obstacle $|\mathbf{s}|$ and summed joint position error $e = \sum_{i=1}^{n} |\tilde{q}_i|$ over time. b) Joint stiffness k and energy tank level over time.

Fig. 8 illustrates the behavior of the adaptive stiffness controller when the robot approaches an obstacle. The stiffness is first lowered by trading-off accuracy in favor of safety and soft joint properties for impact force reduction. During the leaving motion, the distance to the target increases resulting in a rise in stiffness. This period is critical as the rise in stiffness is an active behavior and adds energy to the system, becoming unstable. Since the energy for the stiffness increase is sourced from the energy tank, the system remains stable, which results in stepwise non-continuous progress. The tank limits a further increase in stiffness when the energy is depleted, creating a limited and stepwise increase in stiffness.

VII. Conclusion

In this work, we have demonstrated an approach to improve the safety and accuracy of impedance controlled robot manipulators. The relatively simple approach leverages proximity perception to anticipate impacts to trigger proactive impact reactions within the robot. The reactions modulate the joint stiffness while maintaining overall system stability and allows the robot to switch between high accuracy and safety just as required depending on the situation. The tank-based stability governor tends to create non-continuous stiffness progesses depending on the tank's parameter and the rate of stiffness increase. Kronander et al. [20] proposed an interesting direct relation between damping, stiffness, and stiffness rate for stable behavior without the use of energy tanks. The second mechanism decouples the robot's links from the impact point mechanically, which reduces inertia. Overall, we achieved promising results. They indicate that joint stiffness modulation is very effective, as the stiffness can be reduced very quickly without stability issues. Even systems with small sensing ranges of a few millimeters can benefit from this method, where only the latency and time needed to change the joint parameters are the limitations. On the other hand, safe joint configuration motions only have a minor effect due to quick fast joint acceleration requirements. However, fast acceleration increases risk in unpredictable behavior in changing the whole robot configuration when fully passed through. Therefore, reconfiguration motions require joint constraints where they are only allowed to change within specific ranges and full perception for collision avoidance. Furthermore, instead of maximizing the manipulability, minimizing the effective mass through the mass matrix in the operational space can be investigated.

Appendix I
Manipulability Jacobian

Closed form solution of calculating the proposed manipulability Jacobian $\mathbf{J}_{\mathrm{m_c}}$ for revolute joints:

$$m_{\mathrm{c},i} = \frac{1}{2}\mathbf{j}_{\mathrm{c},i}^{\mathsf{T}}\hat{\mathbf{s}}\hat{\mathbf{s}}^{\mathsf{T}}\mathbf{j}_{\mathrm{c},i} \tag{13}$$

$$\mathbf{J}_{\mathrm{m_c}} = \begin{bmatrix} \frac{\mathrm{d}m_{\mathrm{c},1}}{\mathrm{d}q_1} & \cdots & \frac{\mathrm{d}m_{\mathrm{c},1}}{\mathrm{d}q_n} \\ \vdots & \ddots & \vdots \\ \frac{\mathrm{d}m_{\mathrm{c},n}}{\mathrm{d}q_1} & \cdots & \frac{\mathrm{d}m_{\mathrm{c},n}}{\mathrm{d}q_n} \end{bmatrix} \tag{14}$$

$$\frac{\mathrm{d}m_{\mathrm{c},i}}{\mathrm{d}\mathbf{q}} = \mathbf{j}_{\mathrm{c},i}^{\mathsf{T}}\hat{\mathbf{s}}\hat{\mathbf{s}}^{\mathsf{T}}\frac{\mathrm{d}\mathbf{j}_{\mathrm{c},i}}{\mathrm{d}\mathbf{q}} \tag{15}$$

$$\mathbf{j}_{\mathrm{c},i} = \mathbf{z}_{i\text{-}1} \times (\mathbf{p}_{\mathrm{c}} - \mathbf{p}_{z_{i\text{-}1}}) \tag{16}$$

$$= \mathbf{S}_{\mathbf{z}_{i\text{-}1}}(\mathbf{p}_{\mathrm{c}} - \mathbf{p}_{z_{i\text{-}1}}) \tag{17}$$

$$\frac{\mathrm{d}\mathbf{j}_{\mathrm{c},i}}{\mathrm{d}\mathbf{q}} = \frac{\mathrm{d}\mathbf{S}_{\mathbf{z}_{i\text{-}1}}}{\mathrm{d}\mathbf{q}}(\mathbf{p}_{\mathrm{c}} - \mathbf{p}_{z_{i\text{-}1}}) + \mathbf{S}_{\mathbf{z}_{i\text{-}1}}\left(\mathbf{J}_{\mathrm{p_c}} - \mathbf{J}_{\mathrm{p}_{z_{i\text{-}1}}}\right) \tag{18}$$

$$\frac{\mathrm{d}\mathbf{z}_i}{\mathrm{d}\mathbf{q}} = \begin{bmatrix}\mathbf{z}_0 \times \mathbf{z}_i & \cdots & \mathbf{z}_{i\text{-}1} \times \mathbf{z}_i & 0 & \cdots 0\end{bmatrix} \tag{19}$$

$\mathbf{z}_{i-1}$ is the rotation axis of the i-th joint and $\mathbf{p}_{i-1}$ its position. $\mathbf{p}_{\mathrm{c}}$ is the anticipated contact point. $\mathbf{S}_{\mathbf{z}}$ denotes a skew symmetric matrix to express a cross product as matrix multiplication.

References

[1] G. Pang, G. Yang, W. Heng, Z. Ye, X. Huang, H. Yang, and Z. Pang, "Coboskin: Soft robot skin with variable stiffness for safer human-robot collaboration," *IEEE Transactions on Industrial Electronics*, pp. 1–1, 2020.

[2] N. Hogan, "Impedance control: An approach to manipulation," in *1984 American Control Conference*, 1984, pp. 304–313.

[3] R. Schiavi, A. Bicchi, and F. Flacco, "Integration of active and passive compliance control for safe human-robot coexistence," in *2009 IEEE International Conference on Robotics and Automation*, 2009, pp. 259–264.

[4] A. De Luca, A. Albu-Schaffer, S. Haddadin, and G. Hirzinger, "Collision detection and safe reaction with the dlr-iii lightweight manipulator arm," in *2006 IEEE/RSJ International Conference on Intelligent Robots and Systems*, 2006, pp. 1623–1630.

[5] S. Haddadin, A. Albu-Schaffer, A. De Luca, and G. Hirzinger, "Collision detection and reaction: A contribution to safe physical human-robot interaction," in *2008 IEEE/RSJ International Conference on Intelligent Robots and Systems*, Sep. 2008, pp. 3356–3363.

[6] Y. Ding, F. Wilhelm, L. Faulhammer, and U. Thomas, "With proximity servoing towards safe human-robot-interaction," in *2019 IEEE/RSJ International Conference on Intelligent Robots and Systems (IROS)*, Nov 2019, pp. 4907–4912.

[7] Y. Ding and U. Thomas, "Collision avoidance with proximity servoing for redundant serial robot manipulators," in *2020 IEEE International Conference on Robotics and Automation (ICRA)*, Jun 2020, pp. 4907–4912.

[8] F. Müller, F. Weiske, J. Jäkel, U. Thomas, and J. Suchy, "Human-robot interaction with redundant robots using force-field-dependent variable impedance control," in *2017 IEEE International Symposium on Robotics and Intelligent Sensors (IRIS)*, 2017, pp. 166–172.

[9] F. Ficuciello, L. Villani, and B. Siciliano, "Variable impedance control of redundant manipulators for intuitive human–robot physical interaction," *IEEE Transactions on Robotics*, vol. 31, no. 4, pp. 850–863, 2015.

[10] F. Ferraguti, C. T. Landi, L. Sabattini, M. Bonfè, C. Fantuzzi, and C. Secchi, "A variable admittance control strategy for stable physical human–robot interaction," *The International Journal of Robotics Research*, vol. 38, no. 6, pp. 747–765, 2019.

[11] A. De Luca and F. Flacco, "Integrated control for phri: Collision avoidance, detection, reaction and collaboration," in *2012 4th IEEE RAS EMBS International Conference on Biomedical Robotics and Biomechatronics (BioRob)*, June 2012, pp. 288–295.

[12] R. Z. Stanisic and n. V. Fernández, "Adjusting the parameters of the mechanical impedance for velocity, impact and force control," *Robotica*, vol. 30, no. 4, p. 583–597, 2012.

[13] C. Chun, C. Suh, and S. Kang, "Proximity sensing and reactive control for safe manipulation," in *Proceedings of Australasian Conference on Robotics and Automation*, Dec 2012.

[14] S. Hong, W. Lee, C. Cho, S. Kang, and H. Lee, "Joint configuration strategy for serial-chain safe manipulators," in *2014 IEEE/RSJ International Conference on Intelligent Robots and Systems*, 2014, pp. 2166–2171.

[15] Y. Ding, H. Zhang, and U. Thomas, "Capacitive proximity sensor skin for contactless material detection," in *2018 IEEE/RSJ International Conference on Intelligent Robots and Systems (IROS)*, Oct 2018, pp. 7179–7184.

[16] F. Ferraguti, C. Secchi, and C. Fantuzzi, "A tank-based approach to impedance control with variable stiffness," in *2013 IEEE International Conference on Robotics and Automation*, 2013, pp. 4948–4953.

[17] V. Duindam and S. Stramigioli, "Port-based asymptotic curve tracking for mechanical systems," *European Journal of Control*, vol. 10, no. 5, pp. 411 – 420, 2004.

[18] T. Yoshikawa, "Dynamic manipulability of robot manipulators," in *Proceedings. 1985 IEEE International Conference on Robotics and Automation*, vol. 2, March 1985, pp. 1033–1038.

[19] Y. Nakamura and H. Hanafusa, "Inverse Kinematic Solutions With Singularity Robustness for Robot Manipulator Control," *Journal of Dynamic Systems, Measurement, and Control*, vol. 108, no. 3, pp. 163–171, 09 1986.

[20] K. Kronander and A. Billard, "Stability considerations for variable impedance control," *IEEE Transactions on Robotics*, vol. 32, no. 5, pp. 1298–1305, 2016.